Sign alteration of the nonlinear refraction of isomorphous cubane-shaped heterothiometallic clusters originating from a skeleton atomic effect

Chi Zhang,*[a,b,c] Yinglin Song,[a] Fritz E. Kühn,*[c] Yuxiao Wang,[a] Hoongkun Fun,[e] Xinquan Xin[d] and Wolfgang A. Herrmann*[c]

[a] *Department of Applied Physics, Harbin Institute of Technology, Harbin 150001, P. R. China*
[b] *Department of Chemistry, University of Kansas, Lawrence, KS 66045, USA*
[c] *Anorganisch-Chemisches Institut der Technischen Universität München, Lichtenbergstrasse 4, D-85747 Garching bei München, Germany*
[d] *State Key Laboratory of Coordination Chemistry, Department of Chemistry, Nanjing University, Nanjing 210093, P. R. China*
[e] *X-Ray Crystallography Unit, School of Physics, Universiti Sains Malaysia 11800, USM, Penang, Malaysia*

Received (in New Haven, CT, USA) 29th August 2001, Accepted 4th October 2001
First published as an Advance Article on the web

Employing ligand-redistribution reactions, two heterothiometallic cluster compounds $[MOS_3Cu_3(\mu_3\text{-}X)(2\text{-pic})_3]$ (M = Mo, X = Br, **1**; M = W, X = I, **2**) have been synthesized for third-order excited state nonlinear optical studies. Crystallographic investigations show that clusters **1** and **2** adopt an isomorphous neutral cubane-like skeleton. Such a neutral cubic arrangement with pyridine derivative ligands is found for the first time in heterothiometallic cluster compounds. Their optical nonlinearities were measured by the *Z*-scan technique with a 10 ns pulsed laser at 532 nm. Surprisingly, these two isomorphous clusters exhibit diametrically opposed nonlinear refractive properties, with cluster **1** showing self-defocusing performance (effective nonlinear refractive index $n_2 = -3.8 \times 10^{-18}$ m^2 W^{-1}) and cluster **2** demonstrating a self-focusing effect ($n_2 = 3.5 \times 10^{-17}$ m^2 W^{-1}). Both clusters additionally show strong reverse saturable absorptive abilities. A new nonlinear refraction model is presented to simulate the experimental results. The *Z*-scan experimental results imply that excited state molecules also play a major role in nonlinear refraction. The above NLO refractive properties and absorption abilities suggest that clusters **1** and **2** may be very promising candidates for NLO applications.

The recent great challenge in developing new optical materials with strong excited state nonlinearities has been stimulated by the tremendous interest in their potential applications[1] in optical communications, optical signal processing and transmission, optical switching, optical data acquisition and storage, optical computing, optic-electronic modulation,[2] and especially as optical limiting (OL) materials utilized in the protection of optical sensors and human eyes from high intensity laser beams.[3] The most frequently mentioned materials during the last decade displaying strong excited state nonlinearities are phthalocyanine, fullerene C_{60} and their derivatives.[4,5] In contrast, heterothiometallic cluster compounds with a cubane-type cage or planar 'open' skeleton (similar to that of fullerene or phthalocyanine, respectively) have only recently received increasing attention.[6,7] Two of the key attractive advantages of this kind of material are their large modifiable structures and the presence of many heavy metal atoms in the cluster, resulting in various kinds of nonlinear optical (NLO) functions that can be achieved by manipulation of their structures and alteration of the constituent atoms.

It has also been observed that many excited state absorptive optical materials also possess nonlinear refractive properties that may change the transverse distribution of the beam.[8] Such nonlinear refractive effects may lower the far-field optical power density, and therefore enhance efficiency of optical limiting, if a focusing geometry is employed and an on-axis aperture is positioned in front of the optical sensor. Our previous studies on these heterothiometallic clusters suggest that unlike traditional NLO compounds, both the cluster framework and the skeleton components in these clusters appear to have a considerable influence on the NLO properties. This results in the Mo(W)/S/Cu(Ag) clusters exhibiting rather diverse combinations of NLO effects. The clusters having cubane-like[6] and half-open cubane-like shapes[9] show strong nonlinear absorptions. Large nonlinear refraction effects are found in the nest-shaped[10] and the twin-nest-shaped clusters.[11] The twenty-nuclear supra-cage-shaped cluster possesses a very large nonlinear susceptibility.[8b] The hexagonal prism-shaped clusters,[8c,12] the pentanuclear planar 'open' clusters[7] and cluster polymers[13] seem to reveal large optical limiting properties. Despite the progress that has been made, the discovery of clusters with better and more varied NLO functions remains the bottleneck that slows down the speed of further developing research and applications in the field of nonlinear optics.

In order to further explore this promising field, and also to search for better NLO materials for optical applications, we have synthesized two heterothiometallic cluster compounds

 DOI: 10.1039/b108513c

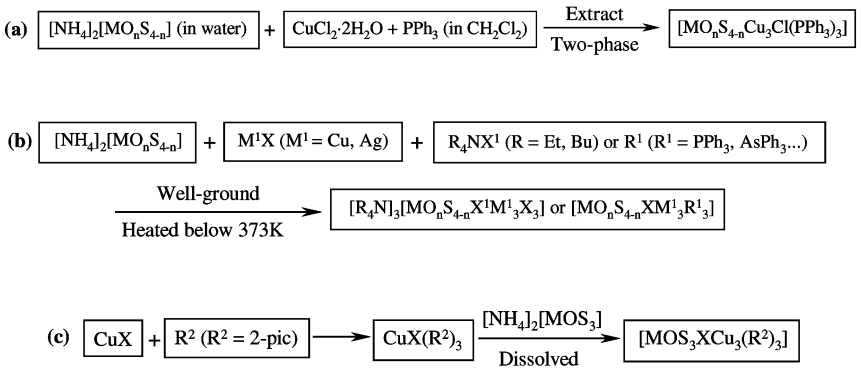

(M = Mo, W; n = 0, 1, 2; X = Cl, Br, I)

Scheme 1

$[MOS_3Cu_3(\mu_3\text{-}X)(2\text{-pic})_3]$ (M = Mo, X = Br, **1**; M = W, X = I, **2**; 2-pic = α-methylpyridine) by a ligand redistribution reaction. The single-crystal X-ray diffraction shows that clusters **1** and **2** are isomorphous and adopt the neutral cubane-like skeleton; such neutral cubic arrangement with pyridine derivative ligands is found in heterothiometallic cluster compounds for the first time. Furthermore, previous NLO research on cubane-shaped clusters has been mainly focused on their optical limiting effects and the NLO absorption performance. However, their NLO refractive functions have never attracted any attention. Surprisingly, these two clusters, having the same cubane-like skeleton but with different central skeleton atoms, show diametrically opposed signs of nonlinear refraction. The *Z*-scan measurements reveal that cluster **1** shows a self-defocusing effect, while cluster **2** exhibits a self-focusing performance. This finding presents a method to alter the nonlinear refraction by using a mixture of two soluble clusters, such as **1** and **2**, with mutually opposite self-lensing effects. The refractive nonlinearity of these clusters can be attributed to an excited state nonlinear refraction effect. A theoretical model of excited state refraction is presented to analyze the experimental results. The results obtained with the theoretical model are in good accordance with the experimental data. The conditions of the sign change of nonlinear refraction have also been studied.

Results and discussion

Preparation and reactions

During the past decades, heterothiometallic cluster compounds with a cubane-like skeleton have aroused great interest for their structural similarity to biological models of some nitrogenases and their large optical limiting properties.[6,14] The typical synthetic routes to tetranuclear cubane-like heterothiometallic clusters have been previously described in two ways.[6,15] In the pioneering work of Muller and co-workers, the so-called two-phase method has been applied by reacting Cu(I)-philic ligands in organic solvent with thiometalate dissolved in water to construct the cubic skeleton clusters [Scheme 1(a)].[15] A low-temperature solid-state synthesis, developed in our laboratory,[6] was also used to prepare cubic clusters by directly reacting the synthon $[MO_nS_{4-n}]^{2-}$ (M = Mo, W; $n = 0$, 1, 2) with starting materials CuX and R_4NX^1 to form the anionic cluster skeleton $[MO_nS_{4-n}Cu_3X^1X_3]^{3-}$, or with CuX and R^1 ($R^1 = PPh_3$, $AsPh_3$,...) ligands to give the neutral cubane-like clusters $[MO_nS_{4-n}Cu_3XR^1{}_3]$ [Scheme 1(b)].[16] However, the yield of the cubane-like clusters with these two methods is very low (13–24% for the former and 10–15% for the latter).

In contrast to the two traditional methods described above, our synthetic approach to prepare the tetranuclear cubane-like clusters, such as **1** and **2**, straightforwardly employing ligand-redistribution reactions in two steps, has proven to be an efficient route. First, the copper complex including mixed ligands was pre-synthesized as the intermediate product, which is not isolated from the reaction system. In our case, the starting material CuX ($X = Br^-$, I^-) reacted with 2-pic, which acts as both the reaction solvent and the σ-donor ligand. Since 2-pic exhibits a strong super-conjugation effect from the methyl group to the pyridine ring, 2-pic has a high tendency to coordinate with Cu atoms. The gradual dissolution of CuX and the formation of a light yellow solution were consistent with the formation of the intermediate product—the Lewis-base adduct $CuX(2\text{-pic})_3$.[17] The second step comprises a ligand substitution reaction; the synthon thiometalate $[MOS_3]^{2-}$ acting as a bidentate ligand was added to the reaction system. The solution immediately turned from light yellow to black– (or orange–) red in color, which suggested that the target cluster compounds were formed. Since the strength of some Cu(I)-philic ligands of Mo(W)/S/Cu(Ag) compounds follows the sequence: $S^{2-} >$ (py, PPh_3) $> X^-$ (X = Cl, Br, I, CN), the former ligands can substitute for part or all of the latter ligands, while the required coordination number of copper(I) is not more than four. Two bonds of $CuX(2\text{-pic})_3$ were broken upon attack by the S^{2-} belonging to the $[MOS_3]^{2-}$ moiety to form the final cubic cluster skeleton [Scheme 1(c)]. Interestingly however, our previous work showed that when we used py or 4-pic as the σ-donor ligand instead of 2-pic to react with CuX ($X = Br^-$, I^-), only the nest-shaped clusters were obtained (Scheme 2).[10a,b,18] This observation may be due to the fact that the presence of py and 4-pic with stronger σ-donor effect [the strength of Cu(I)-philic ligands containing py derivatives follows: 4-pic > py > 2-pic > 3-pic] and less steric inhibition [2-pic > 3-pic > (4-pic, py)] than 2-pic[7] results in py

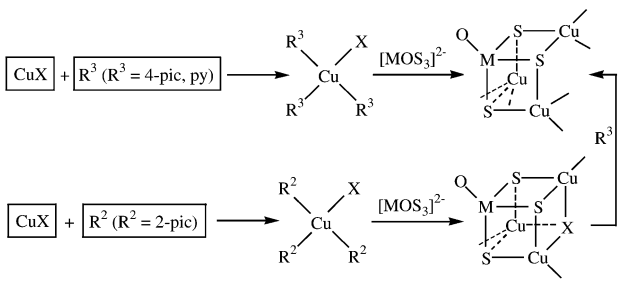

(M = Mo, W; X = Br, I)

Scheme 2

and 4-pic coordination with copper(I). This coordination may be easier than that of 2-pic. To verify our hypothesis, clusters **1** and **2** were further reacted with 4-pic and the 2-pic ligands were successfully substituted by 4-pic, which was confirmed by elemental analysis and IR spectra, and the cubane-like framework of clusters **1** and **2** was accordingly transformed into the nest-shaped skeleton (Scheme 2).

Crystal structure

Selected bond lengths and angles for clusters **1** and **2** are listed in Tables 1 and 2, respectively, with their ORTEP diagrams shown in Fig. 1 and 2. Since the structures of $[MOS_3Cu_3(\mu_3\text{-}X)(2\text{-pic})_3]$ in cluster **1** (M = Mo, X = Br) and **2** (M = W, X = I) are isomorphous, only the structure of cluster **1** is described in detail. Consisting of a ($MoCu_3$) tetrahedron interlocked with a (BrS_3) tetrahedron, the skeleton of the neutral cluster can be described as a slightly distorted cube, in which four corners are occupied by one Br atom and three Cu atoms, with a 2-pic ligand bonding to each Cu atom. Three Cu(2-pic) groups are coordinated to the $[MoOS_3]^{2-}$ unit across three S···S edges. The Mo atom has basically retained the C_{3v} geometry of the free $[MoOS_3]^{2-}$ anion with S–Mo–S(O) angles ranging from 107.09(4)° to 111.60(12)°. The Mo–O(1) bond length in cluster **1** is 1.720(3) Å while the three Mo–S bond lengths are quite similar [2.2685(11)–2.2762(11) Å], consistent with the expected arrangement of one Mo=O double bond and three Mo–S single bonds.

The three Cu atoms are almost equivalent, each is coordinated with two μ_3-S atoms, one μ_3-Br atom and one 2-pic ligand, forming three reverse distorted tetrahedrons. The bond angles of these three Cu atoms are 96.03(3)–123.44(10)° for Cu(1), 95.35(3)–127.14(11)° for Cu(2), and 95.06(3)–126.40(11)° for Cu(3). The Mo–Cu lengths, ranging from 2.6687(6) to 2.6838(6) Å, are slightly longer than those in $[Et_4N]_3[MoOS_3(\mu_2\text{-}Br)(CuBr)_3]$ [2.645(3)–2.663(2) Å],[9a] but are significantly shorter than those in $[MoOS_3Cu_3Cl(PPh_3)_3]$ [2.705(2)–2.740(2) Å].[15] The Cu–S distances, varying from 2.2735(12) to 2.2812(11) Å, are obviously longer than those in $[Bu_4N]_2[MoOS_3Cu_3BrCl_2]$ [2.230(3)–2.243(2) Å][10c] and fall in the same range as those found in $[MoOS_3Cu_3(PPh_3)_3(S_2P(OBu)_2)]$ [2.266(5)–2.331(6) Å][19] and $[MoOS_3Cu_3Cl(PPh_3)_3]$ [2.277(5)–2.322(5) Å].[15] The bond distance of Cu(2)–Br(1) [2.8564(8) Å] is slightly shorter than that of the Cu(1)–Br(1) bond [2.8888(8) Å] and the Cu(3)–Br(1) bond [2.8640(8) Å], while the three Cu–N bond lengths are almost the same. From the bond lengths of Cu–S and Cu–Br, we can also conclude that the coordination of the Cu(2) atom with the S(1)···S(2) edge and the Br(1) atom is stronger than that of the Cu(1) atom with the S(1)···S(3) edge and the Br(1) atom. The same is true for the Cu(3) atom with the S(2)···S(3) edge and the Br(1) atom, although all three Cu atoms have the same coordination mode, namely CuS_2Br(2-pic).

Table 1 Selected bond lengths (Å) and angles (°) for cluster $[MoOS_3Cu_3Br(2\text{-pic})_3]$, **1**

Br(1)–Cu(2)	2.8564(8)	Cu(1)–N(3)	1.978(3)
Br(1)–Cu(3)	2.8640(8)	Cu(1)–S(1)	2.2735(12)
Br(1)–Cu(1)	2.8888(8)	Cu(1)–S(3)	2.2809(12)
Mo–O(1)	1.720(3)	Cu(2)–N(2)	1.978(3)
Mo–S(1)	2.2685(11)	Cu(2)–S(1)	2.2743(12)
Mo–S(3)	2.2739(10)	Cu(2)–S(2)	2.2771(12)
Mo–S(2)	2.2762(11)	Cu(3)–N(1)	1.980(4)
Mo–Cu(2)	2.6687(6)	Cu(3)–S(3)	2.2747(12)
Mo–Cu(3)	2.6719(6)	Cu(3)–S(2)	2.2812(11)
Mo–Cu(1)	2.6838(6)		
Cu(2)–Br(1)–Cu(3)	70.261(19)	N(2)–Cu(2)–Br(1)	107.40(10)
Cu(2)–Br(1)–Cu(1)	69.457(18)	S(1)–Cu(2)–Br(1)	96.90(4)
Cu(3)–Br(1)–Cu(1)	68.870(19)	S(2)–Cu(2)–Br(1)	95.35(3)
O(1)–Mo–S(1)	111.03(12)	N(1)–Cu(3)–S(3)	119.38(11)
O(1)–Mo–S(3)	111.60(12)	N(1)–Cu(3)–S(2)	126.40(11)
S(1)–Mo–S(3)	107.09(4)	S(3)–Cu(3)–S(2)	107.41(4)
O(1)–Mo–S(2)	111.52(12)	N(1)–Cu(3)–Br(1)	102.48(12)
S(1)–Mo–S(2)	107.78(4)	S(3)–Cu(3)–Br(1)	97.94(4)
S(3)–Mo–S(2)	107.61(4)	S(2)–Cu(3)–Br(1)	95.06(3)
N(3)–Cu(1)–S(1)	123.44(10)	Mo–S(1)–Cu(1)	72.44(3)
N(3)–Cu(1)–S(3)	123.13(10)	Mo–S(1)–Cu(2)	71.95(3)
S(1)–Cu(1)–S(3)	106.68(4)	Cu(1)–S(1)–Cu(2)	92.06(4)
N(3)–Cu(1)–Br(1)	102.14(10)	Mo–S(2)–Cu(2)	71.76(3)
S(1)–Cu(1)–Br(1)	96.03(3)	Mo–S(2)–Cu(3)	71.79(3)
S(3)–Cu(1)–Br(1)	97.10(4)	Cu(2)–S(2)–Cu(3)	92.46(4)
N(2)–Cu(2)–S(1)	115.85(10)	Mo–S(3)–Cu(3)	71.95(3)
N(2)–Cu(2)–S(2)	127.14(11)	Mo–S(3)–Cu(1)	72.20(3)
S(1)–Cu(2)–S(2)	107.55(4)	Cu(3)–S(3)–Cu(1)	91.14(4)

Table 2 Selected bond lengths (Å) and angles (°) for cluster $[WOS_3Cu_3I(2\text{-pic})_3]$, **2**

W(1)–O(1)	1.776(8)	Cu(1)–N(1)	1.977(9)
W(1)–S(1)	2.255(3)	Cu(1)–S(2)	2.286(4)
W(1)–S(2)	2.258(3)	Cu(1)–S(1)	2.294(3)
W(1)–S(3)	2.257(3)	Cu(2)–N(2)	1.996(10)
W(1)–Cu(1)	2.6758(18)	Cu(2)–S(1)	2.294(4)
W(1)–Cu(3)	2.6863(17)	Cu(2)–S(3)	2.320(4)
W(1)–Cu(2)	2.7056(17)	Cu(3)–N(3)	1.989(11)
I(1)–Cu(2)	2.972(2)	Cu(3)–S(2)	2.294(4)
I(1)–Cu(1)	2.986(2)	Cu(3)–S(3)	2.303(4)
I(1)–Cu(3)	2.996(2)		
O(1)–W(1)–S(1)	110.1(3)	S(1)–Cu(2)–S(3)	104.47(13)
O(1)–W(1)–S(2)	110.8(3)	N(2)–Cu(2)–I(1)	103.1(3)
S(1)–W(1)–S(2)	108.48(11)	S(1)–Cu(2)–I(1)	98.35(10)
O(1)–W(1)–S(3)	111.1(3)	S(3)–Cu(2)–I(1)	98.94(10)
S(1)–W(1)–S(3)	107.85(12)	N(3)–Cu(3)–S(2)	124.6(3)
S(2)–W(1)–S(3)	108.47(12)	N(3)–Cu(3)–S(3)	121.5(3)
Cu(2)–I(1)–Cu(1)	66.85(5)	S(2)–Cu(3)–S(3)	105.68(12)
Cu(2)–I(1)–Cu(3)	66.78(5)	N(3)–Cu(3)–I(1)	103.4(4)
Cu(1)–I(1)–Cu(3)	67.61(5)	S(2)–Cu(3)–I(1)	95.89(10)
N(1)–Cu(1)–S(2)	127.7(3)	S(3)–Cu(3)–I(1)	98.65(10)
N(1)–Cu(1)–S(1)	115.3(3)	W(1)–S(1)–Cu(1)	72.05(10)
S(2)–Cu(1)–S(1)	106.19(13)	W(1)–S(1)–Cu(2)	72.97(10)
N(1)–Cu(1)–I(1)	107.5(3)	Cu(1)–S(1)–Cu(2)	91.34(12)
S(2)–Cu(1)–I(1)	96.37(10)	W(1)–S(2)–Cu(1)	72.16(10)
S(1)–Cu(1)–I(1)	97.98(10)	W(1)–S(2)–Cu(3)	72.33(10)
N(2)–Cu(2)–S(1)	123.3(3)	Cu(1)–S(2)–Cu(3)	93.22(13)
N(2)–Cu(2)–S(3)	122.7(3)	W(1)–S(3)–Cu(3)	72.18(9)
Cu(3)–S(3)–Cu(2)	90.57(12)	W(1)–S(3)–Cu(2)	72.46(10)

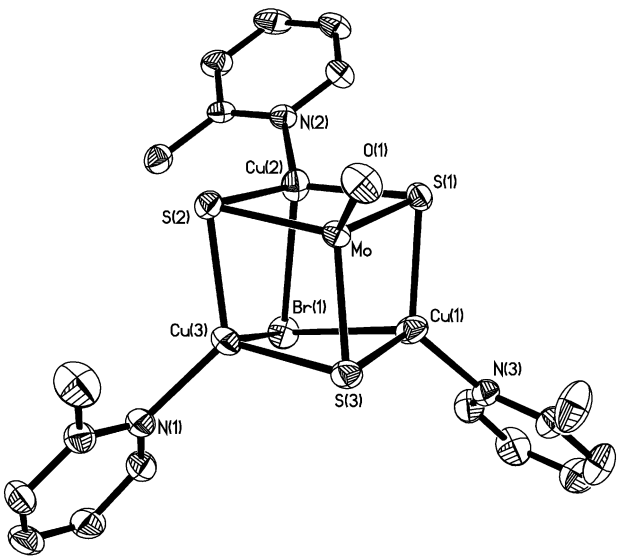

Fig. 1 A perspective view of the structure of the neutral cluster $[MoOS_3Cu_3Br(2\text{-pic})_3]$, **1**.

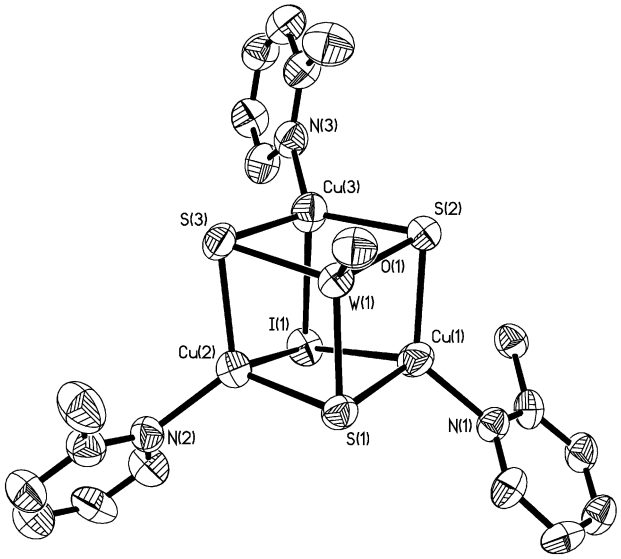

Fig. 2 A perspective view of the structure of the neutral cluster $[WOS_3Cu_3I(2\text{-pic})_3]$, **2**.

Third-order optical nonlinearities

Previous NLO investigations on cubane-like shaped clusters were largely devoted to exploring their optical limiting effects and the NLO absorption performance;[6] their NLO refractive functions seem to have been generally neglected for a long time. In this report, the excited state optical nonlinearities of clusters **1** and **2** for a 10 ns pulse width was determined by an open-aperture *Z*-scan measurement.[20] The optical performances of nonlinear absorption and refraction are shown in Fig. 3 and 4, for clusters **1** and **2**, respectively. Fig. 3(a) and 4(a) depict the *Z*-scan experimental results under the open-aperture configuration for the nonlinear absorptive component of clusters **1** and **2**, while Fig. 3(b) and 4(b) show those obtained by dividing the closed-aperture data by the open-aperture data to effectively eliminate the absorptive effect and reveal the nonlinear refractive behavior of clusters **1** and **2**. The nonlinear refraction is found to have a negative sign for cluster **1** and a positive sign for cluster **2**, with the effective n_2 values of -3.8×10^{-18} m^2 W^{-1} for cluster **1** and 3.5×10^{-17} m^2 W^{-1} for cluster **2**, derived from the theoretical curves. Obviously, cluster **1** demonstrates a self-defocusing performance, while cluster **2** displays a self-focusing effect. To make a comparison of the NLO refractive effects, the effective n_2 values of clusters **1** and **2**, as well as other different structural clusters such as nest-shaped,[10] butterfly-shaped,[21] half-open cubane-shaped,[9] twin-nest-shaped,[11] hexagonal-prism-shaped,[8c,12] linear-shaped,[22] twenty-nuclear cage-shaped,[8b] planar 'open' shaped,[7] and 3-D cluster polymers[13] are listed in Table 3. The change in transmittance is very large in the open-aperture case [Fig. 3(a) or 4(a)], which indicates that these two clusters have a strong excited state absorption, or a reverse saturable absorption (RSA), at 532 nm.

It is well-known that the origin of excited state optical nonlinearity in molecules is related to the intensity-dependent population distribution of excited states. The nonlinear absorption of materials includes molecular absorption in each energy level. The nonlinear refraction of materials is similar to the nonlinear absorption in that it also results from the energy-level transitions in molecules. Each molecular level can be characterized by an absorption cross-section and by an index of refraction. So the complex intensity-dependent index of refraction for molecules can be written as:[23]

$$\eta(I) = \sum_i N_i\eta_i + i(\lambda/4\pi)\sum_i N_i\sigma_i \qquad (1)$$

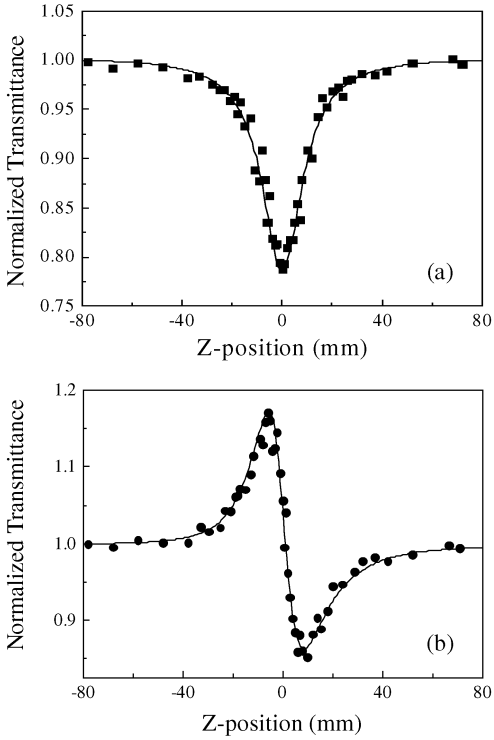

Fig. 3 *Z*-scan measurement of cluster **1** in 6.2×10^{-4} mol dm^{-3} DMF solution. (a) The data collected under the open-aperture configuration; (b) the data obtained by dividing the normalized *Z*-scan data obtained under the closed-aperture configuration by the normalized *Z*-scan data in (a). The filled symbols represent the *Z*-scan experimental results and the solid curves are the theoretical fits based on *Z*-scan theoretical calculations. The input energy is 220 μJ.

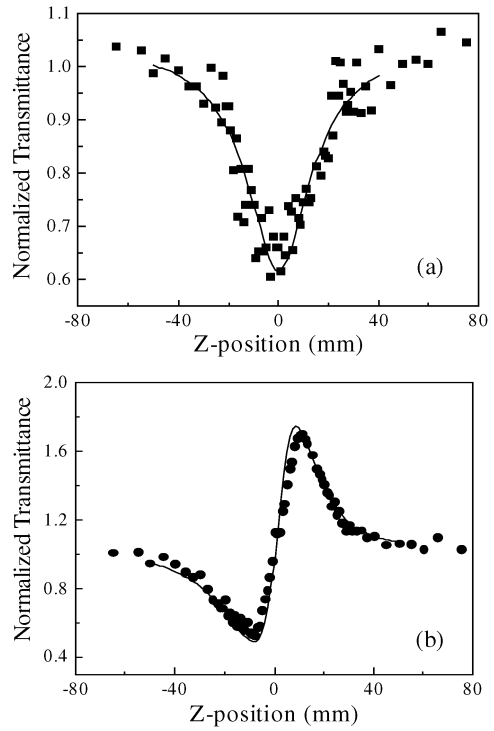

Fig. 4 *Z*-scan measurement of cluster **2** in 5.3×10^{-4} mol dm^{-3} DMF solution. (a) The data collected under the open-aperture configuration; (b) the data obtained by dividing the normalized *Z*-scan data obtained under the closed-aperture configuration by the normalized *Z*-scan data in (a). The filled symbols represent the *Z*-scan experimental results and the solid curves are the theoretical fits based on *Z*-scan theoretical calculations. The input energy is 220 μJ.

Table 3 Nonlinear optical refractive values of the heterothiometallic cluster compounds measured at 532 nm with ns laser pulses

Compound	Structure type	n_2/m^2 W^{-1}	N/mol dm^{-3}	Ref.
$[MoOS_3Cu_2(PPh_3)_3]$	Butterfly	5.0×10^{-17}	7.4×10^{-5} [a]	21
$[WOS_3Cu_2(PPh_3)_4]$	Butterfly	8.0×10^{-18}	1.2×10^{-4} [a]	21
$[Et_4N]_3[MoOS_3(CuBr)_3(\mu_2\text{-Br})]$	Half-open cubane-like	-2.3×10^{-16}	1.9×10^{-3} [a]	9(*a*)
$[Et_4N]_3[WOS_3(CuI)_3(\mu_2\text{-I})]$	Half-open cubane-like	-3.0×10^{-17}	2.3×10^{-4} [a]	9(*c*)
$[MoAu_2S_4(AsPh_3)_2]$	Linear	5.1×10^{-17}	6.4×10^{-4} [b]	22
$[WAu_2S_4(AsPh_3)_2]$	Linear	1.0×10^{-16}	5.4×10^{-4} [b]	22
$[Mo_2Ag_4S_8(PPh_3)_4]$	Hexagonal prism	2.2×10^{-16}	1.3×10^{-4} [c]	8(*c*)
$[MoOS_3Cu_3(4\text{-pic})_6] \cdot 0.5[Mo_2O_7]$	Nest	1.7×10^{-16}	3.52×10^{-4} [a]	10(*a*)
$[WOS_3Cu_3(4\text{-pic})_6] \cdot 0.5[W_2O_7]$	Nest	1.0×10^{-16}	2.67×10^{-4} [a]	10(*a*)
$[MoOS_3Cu_3(4\text{-pic})_6] \cdot BF_4$	Nest	9.0×10^{-17}	4.82×10^{-4} [a]	10(*a*)
$[WOS_3Cu_3(4\text{-pic})_6] \cdot BF_4$	Nest	8.2×10^{-18}	3.75×10^{-4} [a]	10(*a*)
$[Et_4N]_4[Mo_2O_2S_6Cu_6I_6]$	Twin-nest	-6.0×10^{-17}	2×10^{-3} [a]	11(*a*)
$[n\text{-}Bu_4N]_4[Mo_8Cu_{12}O_8S_{24}]$	Twenty-nuclear cage	-3.5×10^{-16}	8.0×10^{-4} [b]	8(*b*)
$\{[Et_4N]_2[MoS_4Cu_4(CN)_4]\}_n$	3-D cluster polymer	1.8×10^{-16}	3.64×10^{-5} [d]	13(*a*)
$\{[Et_4N]_2[WS_4Cu_4(CN)_4]\}_n$	3-D cluster polymer	1.2×10^{-16}	2.93×10^{-5} [d]	13(*a*)
$[Et_4N]_2[MoS_4Cu_4(SCN)_4(2\text{-pic})_4]$	Planar 'open'	-8.5×10^{-16}	7.44×10^{-4} [d]	7(*b*)
$[Et_4N]_2[WS_4Cu_4(SCN)_4(2\text{-pic})_4]$	Planar 'open'	-6.8×10^{-16}	6.98×10^{-4} [d]	7(*b*)
$[MoS_4Cu_4Br_2(py)_6]$	Planar 'open'	1.8×10^{-16}	3.8×10^{-4} [d]	7(*c*)
$[WS_4Cu_4Br_2(py)_6]$	Planar 'open'	1.1×10^{-16}	2.83×10^{-4} [d]	7(*c*)
$[MoS_4Cu_4I_2(py)_6]$	Planar 'open'	2.5×10^{-16}	1.39×10^{-4} [d]	7(*c*)
$[WS_4Cu_4I_2(py)_6]$	Planar 'open'	1.2×10^{-16}	5.5×10^{-4} [d]	7(*c*)
$[MoOS_3Cu_3Br(2\text{-pic})_3]$	Cubane-like	-3.8×10^{-18}	6.2×10^{-4} [d]	This work
$[WOS_3Cu_3I(2\text{-pic})_3]$	Cubane-like	3.5×10^{-17}	5.3×10^{-4} [d]	This work

[a] In CH_3CN. [b] In CH_2Cl_2. [c] In acetone. [d] In DMF.

where λ is the wavelength, η_i, σ_i and N_i are the refraction volume (which will be defined in the following discussion), the absorption cross-section and the population of each level, respectively.

In our Z-scan experiments, the input energy is not high and the laser pulse width is longer than the lifetime of the excited state level, which is usually on the order of hundreds of picoseconds. This enables us to apply the steady-state nonlinear absorption theory, which describes RSA by using a two-energy-level model.[23] Then the equation for the intensity of a laser beam propagating (along the positive z direction) through a nonlinear medium can be written as:[5c]

$$\frac{dI}{dz} = -\alpha I \tag{2}$$

where α is the nonlinear absorption coefficient that describes RSA by using a two-energy-level model, which can be expressed as a function of the incident pulsed light intensity I:[5c]

$$\alpha = \alpha_0 + \frac{1 + K_\alpha \frac{I}{I_s}}{1 + \frac{I}{I_s}} \sigma_0 N \tag{3}$$

α_0 is the linear absorptive coefficient, $I_s = \hbar\nu/\sigma_0\tau_{s0}$ is the saturable intensity, N is the concentration of the cluster sample solution, and $K_\alpha = \sigma_s/\sigma_0$ is the ratio of the excited state absorption cross-section to the ground state absorption cross-section. If $K_\alpha > 1$, the medium displays a reverse saturable absorption. By contrast, if $K_\alpha < 1$, only a saturable absorption effect occurs.

Based on the discussion above, the Z-scan measurements[20] have been therefore conducted on clusters **1** and **2** by using TEM00 mode laser pulses, which have a beam waist radius of ω_0, a Gaussian temporal profile of duration τ, and a propagation direction along positive z. The irradiance I thus varies with z, r, and t as:[24]

$$I(z, r, t) = \frac{\omega_0^2}{\omega^2(z)} I_{00} \exp\left[-\left(\frac{t}{\tau}\right)^2\right] \exp\left[-\left(\frac{2r^2}{\omega^2(z)}\right)\right] \tag{4}$$

where $\omega(z) = \omega_0[1 + (z/z_0)^2]^{1/2}$ is the beam radius at z, $z_0 = \pi\omega_0{}^2/\lambda$ is the diffraction length of the beam, and I_{00} is the on-axis peak irradiance at focus. The parameters of the absorption cross-sections of the ground and excited states are listed in Table 4. Theoretical fits to our experimental results are shown in Fig. 3(a) and 4(a) as solid lines. It is obvious that the theoretical calculations agree well with our experimental results. The parameters of these clusters are obtained from the theoretical analysis. The saturable intensity I_s and coefficient K_α are calculated to be $I_s = 1.5 \times 10^8$ W cm^2 and $K_\alpha = 4.0$ and 8.0 for clusters **1** and **2**, respectively. The absorption cross-section of the ground state is known to be $\sigma_{01} = 3.22 \times 10^{-18}$ cm^2 and $\sigma_{02} = 1.24 \times 10^{-18}$ cm^2 for clusters **1** and **2**, respectively. Therefore, we can finally obtain the excited state absorption cross-sections to be $\sigma_{s1} = 12.9 \times 10^{-18}$ cm^2 and $\sigma_{s2} = 9.92 \times 10^{-18}$ cm^2 for clusters **1** and **2**, respectively.

On the other hand, generally the nonlinear refraction can be described by a Kerr type effect (*i.e.*, $\Delta n = \gamma I$).[25] However, for the excited state nonlinear optical effect, we find that the excited state nonlinear refraction cannot be well interpreted as a Kerr effect. In order to explain such nonlinear refraction phenomenon of clusters **1** and **2**, eqn. (1) must be introduced, and therefore the total refractive index of a multi-level molecular system in the low-intensity case is equal to the sum of the linear refractive index of the solvent n_0 and the nonlinear refractive indices arising from all possible energy level transitions. The refractive index due to each transition is proportional to the population difference between two levels, where we define the constant of proportionality, the refractive volume, as η_n. For our two-energy-level model, the nonlinear index n can be represented as:[26]

Table 4 The parameters of the absorption cross-section and the refraction volume of both the ground and the excited states

	Cluster **1**	Cluster **2**
$\sigma_0/10^{-18}$ cm^2	3.22	1.24
$\sigma_s/10^{-18}$ cm^2	12.9	9.92
K_α	4.0	8.0
$\eta_0/10^{-22}$ cm^3	1.17	1.17
$\eta_s/10^{-22}$ cm^3	0.59	2.34
K_r	0.5	2.0

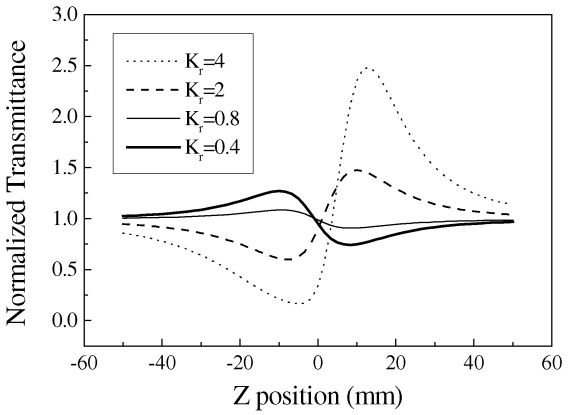

Fig. 5 Theoretical curves for different K_r values.

$$n = n_0 + \eta_0 N_0 + \eta_S N_S \quad (5)$$

When all the molecules are in the ground state, $n_{0s} = n_0 + \eta_0 N$ is the linear refractive index of the solution. For the sake of simplicity, we only consider the case of steady state. In this case, we can obtain eqn. (6):[26]

$$n = n_0 + \frac{1 + k_r \frac{I}{I_s}}{1 + \frac{I}{I_s}} \eta_0 N \quad (6)$$

where $K_r = \eta_s/\eta_0$ is the ratio of the refraction volume of the excited state to that of the ground state.

Based on eqns. (4) and (6), as well as on the standard theory of the *Z*-scan technique,[20] we can describe the relationship between the ratio of the refractive volumes and the sign of the nonlinear refraction. We calculated the refraction index change in the cases of $K_r = 4$, 2, 0.8, and 0.4. The results are shown in Fig. 5. When K_r is larger than 1, the behavior is self-focusing; when K_r is less than 1, self-defocusing will be observed. Such a model was used to study the nonlinear optical properties of the heterothiometallic clusters **1** and **2**, and successfully fit our experimental results, which are shown in Fig. 3(b) and 4(b) as solid lines. The ratio K_r is calculated to be 0.5 from the fitted curve for cluster **1** and 2.0 for cluster **2**. The refraction volume of the ground state is $\eta_0 = 1.17 \times 10^{-22}$ cm^3, which is calculated from n_{0s}. Finally, we can obtain the excited state refraction volume $\eta_{s1} = 0.59 \times 10^{-22}$ cm^3 for cluster **1** and $\eta_{s2} = 2.69 \times 10^{-22}$ cm^3 for cluster **2**.

Conclusions

We have synthesized and characterized two isomorphous heterothiometallic clusters **1** and **2**, with the same cubane-like skeleton and different central skeleton atoms. Such a neutral cubic arrangement with pyridine derivative ligands is found for the first time in heterothiometallic cluster compounds. The different synthetic routes to cubane-like shaped clusters were formulated, based on the reactivity of the trithiometalate, and have been discussed and compared with each other.

The skeleton atomic effect on the NLO refractive performance has been studied. A small alteration in the central skeleton atoms may lead to diametrically different nonlinear refractive properties, with cluster **1** showing a self-defocusing effect and cluster **2** exhibiting a self-focusing property. Such opposing behavior make these two clusters with a neutral cubic skeleton very attractive for nonlinear optical applications. The *Z*-scan technique was applied to investigate the optical nonlinearity, the reverse saturable absorption and the excited state nonlinear refraction of DMF solutions of clusters **1** and **2**. A new nonlinear refraction model is presented to simulate the experimental results. Some parameters were obtained from these theoretical calculations. These experiments imply that excited state molecules also play a major role in nonlinear refraction. The ratio of the excited state absorption cross-section to the ground state absorption cross-section K_α is 4.0 and 8.0 for clusters **1** and **2**, respectively. When the ratio of refraction volumes of the excited state to that of the ground state $K_r > 1$, the behavior is self focusing and self-defocusing when $K_r < 1$. Such a study opens up possibilities to further explore and establish the structure-function relationships of these kinds of NLO materials, and can be helpful to synthesize still better materials with strong NLO properties or various NLO functions through rational molecular structure design.

Experimental

Materials and methods

All reactions and manipulations were conducted using standard Schlenk techniques under an atmosphere of nitrogen. The compounds $(NH_4)_2MOS_3$ (M = Mo, W) were prepared according to literature procedures.[27] Solvents were carefully dried and distilled prior to use, and all other chemicals were used as commercially available.

Elemental analysis for carbon, hydrogen and nitrogen were performed on a Perkin–Elmer 240C elemental analyzer. Infrared spectra were recorded with a Nicolet FT-170SX Fourier transform spectrometer (KBr pellets). Electronic spectra were measured on a Shimadzu UV-3100 spectrophotometer.

Syntheses

Preparation of cluster $[MoOS_3Cu_3(\mu_3\text{-}Br)(2\text{-}pic)_3]$, 1. CuBr (3 mmol, 0.431 g) was added to 20 mL 2-pic and the solution was stirred for *ca.* 5 min. at room temperature. Then $(NH_4)_2MoOS_3$ (1 mmol, 0.244 g) was added. The reaction system immediately changed color to black-red and was stirred for an additional 10 min. The resulting solution was subsequently filtered to afford a black-red filtrate. Black–red crystals (0.322 g; yield: 42.5%) were obtained after several days by layering the filtrate with *i*-PrOH. Anal. calcd. for $MoOS_3Cu_3BrC_{18}H_{21}N_3$ (%): C, 28.5; H, 2.8; N, 5.5; found: C, 28.6; H, 2.9; N, 5.7%. UV-vis [DMF, λ_{max}/nm, 10^3 ε/cm^{-1} mol^{-1} dm^3)]: 495 (5.2), 376 (10.2), 311 (19.9). IR (KBr pellet; cm^{-1}): 1603(vs), 1483(s), 902(vs) ν(Mo–O_t), 754(vs), 447(vs) ν(Mo–μ_3-S).

Preparation of cluster $[WOS_3Cu_3(\mu_3\text{-}I)(2\text{-}pic)_3]$, 2. The same procedure as in the preparation of cluster **1** was employed to synthesize cluster **2** except that CuI (3 mmol, 0.571 g) was used instead of CuBr (3 mmol) and $(NH_4)_2WOS_3$ (1 mmol, 0.332 g) was used instead of $(NH_4)_2MoOS_3$ (1 mmol). Deep-red crystals (0.556 g; yield: 62.3%) were obtained. Anal. calcd. for $WOS_3Cu_3IC_{18}H_{21}N_3$ (%): C, 24.2; H, 2.4; N, 4.7; found: C, 24.1; H, 2.3; N, 4.8. UV-vis [DMF, λ_{max}/nm, (10^3 ε/cm^{-1} mol^{-1} dm^3)]: 427 (5.7), 324 (14.4), 293 (19.7). IR (KBr pellet; cm^{-1}): 1602(vs), 1483(vs), 917(vs) ν(W–O_t), 753(vs), 437(vs) ν(W–μ_3-S).

Reactions of clusters 1 and 2 with 4-pic. The above described crystals of clusters **1** or **2** (0.379 g, 0.5 mmol of **1**; 0.447 g, 0.5 mmol of **2**) were added to 4-pic (15 mL). The mixture was stirred for 2 h at *ca.* 60 °C such that the crystalline compounds were completely dissolved. Stirring was continued for another 2 h at room temperature, and then the mixture was filtered to afford a red (or orange–red) filtrate. The filtrate was layered with *i*-PrOH and black-red crystals

of **3** or orange–red crystals of **4** were obtained after several days. The product was washed with EtOH and Et_2O and dried under vacuum. Yield: 0.161 g (31%) **3**, 0.246 g (42%) **4**. These two compounds were identified as having the tetranuclear nest-shaped skeleton $[MOS_3Cu_3(4\text{-pic})_6]^+$ (M = Mo, **3**; W, **4**) by using spectroscopic methods and elemental analyses. **3**: Anal. calcd. for $MoOS_3Cu_3C_{36}H_{42}N_6Br$ (%): C, 41.7; H, 4.1; N, 8.1; found: C, 41.5; H, 4.0; N, 8.3%. IR (KBr pellet, cm^{-1}): 1614(vs), 1421(s), 910(vs) ν(Mo–O_t), 813(vs), 492(vs), 437(vs) ν(Mo–μ_3-S). **4**: Anal. calcd. for $WOS_3Cu_3C_{36}H_{42}N_6I$ (%): C, 36.9; H, 3.6; N, 7.2; found: C, 36.6; H, 3.5; N, 7.0%. IR (KBr pellet, cm^{-1}): 1614(vs), 1420(s), 924(vs) ν(W–O_t), 813(vs), 492(vs), 428(vs) ν(W–μ_3-S).

Crystal structure determinations

A well-developed single crystal of cluster **1** or **2** with suitable dimensions was mounted on a glass fiber. The diffraction data of **1** were collected at 20 ± 2 °C on a Siemens Smart CCD area-detector diffractometer by using an ω-scan technique. The data reductions of **1** were performed on a Silicon Graphics Indy workstation with SAINT-CCD software. The diffraction data of **2** were collected on a Siemens P4 four-circle diffractometer with unit cell parameters determined from automatic centering of 25 reflections by least-squares methods. The data were corrected for Lorentz and polarization effects during data reduction using XSCANS. Both structures of **1** and **2** were solved by the direct methods and refined by full-matrix least-squares on F^2 using the SHELXTL-PC (version 5.1) package of crystallographic software.[28] All non-hydrogen atoms were refined anisotropically by full-matrix least-squares methods. The hydrogen atoms were placed in their calculated positions, fixed isotropic thermal parameters were assigned and riding on their respective parent atoms were allowed. Data processing and structure refinement parameters are listed in Table 5.

CCDC reference numbers 162907 and 162908. See http://www.rsc.org/suppdata/nj/b1/b108513c/ for cyrstallographic data in CIF or other electronic format.

Optical measurements

The third-order NLO absorptive and refractive properties of the cluster solutions of **1** and **2** were measured by the *Z*-scan technique[20] at 532 nm, using a Continuum ns/ps Nd:YAG laser system with a pulse width of 10 ns at a 1 Hz repetition rate. The clusters are stable toward air and laser light under the experimental conditions. The spatial profiles of the optical pulses were of nearly Gaussian transverse mode. The pulsed laser was focused onto the sample cell with a 20 cm focal length mirror. The energies of the input and output pulses were measured simultaneously by precision laser detectors (Rjp-735 energy probes) that were linked to a computer by an IEEE interface,[29] while the incident pulse energy was varied by a Newport Co. attenuator. The experimental data were collected utilizing a single shot at a rate of 1 pulse per minute to avoid the influence of thermal effects. The samples were mounted on a translation stage that was controlled by the computer to move along the axis of the incident laser beam (*Z* direction) with respect to the focal point instead of being positioned at its focal point. To determine both the sign and magnitude of the nonlinear refraction, a 0.2 mm diameter aperture was placed in front of the transmission detector and the transmittance recorded as a function of the sample position on the *Z* axis (closed-aperture *Z*-scan). To measure the nonlinear absorption, the *Z*-dependent sample transmittance was taken without the aperture (open-aperture *Z*-scan). The linear transmittance of the samples is 90% for **1** and 95% for **2** separately, at the input energy of 220 μJ.

Table 5 Crystal data and structure refinement for $[MoOS_3Cu_3Br(2\text{-pic})_3]$, **1**, and $[WOS_3Cu_3I(2\text{-pic})_3]$, **2**

	1	**2**
Chemical formula	$C_{18}H_{21}Cu_3BrN_3OS_3Mo$	$C_{18}H_{21}Cu_3IN_3OS_3W$
Formula weight	758.03	892.93
Temperature/K	293(2)	293(2)
Wavelength/Å	0.71073	0.71073
Crystal system	Orthorhombic	Orthorhombic
Space group	$P2_12_12_1$	$P2_12_12_1$
a/Å	11.1287(5)	11.968(5)
b/Å	11.9739(5)	19.102(4)
c/Å	18.9832(8)	11.209(2)
$\alpha=\beta=\gamma$/°	90	90
U/Å^3	2529.59(19)	2529.59(19)
Z	4	4
$\mu\mu$/mm^{-1}	4.815	8.395
Reflections collected	18 246	3315
Reflections unique	6373	3116
R_{int}	0.0668	0.0299
$R_1[I > 2\sigma(I)]$	0.0324	0.0358
$wR_2[I > 2\sigma(I)]$	0.0646	0.0886
R_1 (all data)	0.0453	0.0426
wR_2 (all data)	0.0682	0.0941

Acknowledgements

Dr C. Zhang greatly appreciates the Alexander von Humboldt Foundation for awarding a Humboldt Research Fellowship. Financial support from the National Science Foundations of China and USA, the Foundations of the Harbin Institute of Technology and the Universiti Sains Malaysia is acknowledged. The authors are grateful to Dr Douglas R. Powell for helpful discussions.

References

1 (*a*) *Molecular Nonlinear Optics*, ed. J. Zyss, Academic Press, New York, 1994; (*b*) *Nonlinear Optics of Organic Molecules and Polymers*, ed. H. S. Nalwa and S. Miyata, CRC Press, New York, 1997.

2 (*a*) A. Miller, K. R. Welford and B. Daino, *Nonlinear Optical Materials and Devices*, Kluwer Academic Publishers, Dordrecht, The Netherlands, 1993; (*b*) S. P. Karna and A. T. Yeates, *Nonlinear Optical Materials*, American Chemical Society, Washington, DC, 1996; (*c*) S. R. Marder, B. Kippelen, A. K. Y. Jen and N. Peyghambarian, *Nature (London)*, 1997, **388**, 845; (*d*) R. Syms and J. Cozens, *Optical Guided Waves and Devices*, McGraw-Hill, London, 1993; (*e*) I. R. Whittall, A. M. McDonagh, M. G. Humphrey and M. Samoc, *Adv. Organomet. Chem.*, 1999, **43**, 349.

3 (*a*) *Conference on Laser and Electro-optics*, Technical Digest Series, Optical Society of America, Washington, DC, 1993; (*b*) S. R. Marder, J. E. Sohn and G. D. Strucky, *Materials for Nonlinear Optics, Chemical Perspectives*, American Chemical Society, Washington DC, 1991; (*c*) D. J. Hagan, T. Xia, A. Dogariu, A. A. Said and E. W. van Stryland, *MRS Symp. Proc. (Materials for Optical Limiting)*, 1995, 374; (*d*) R. Sutherland, R. Pachter, P. Hood, D. J. Hagan, K. Lewis and J. W. Perry, *MRS Symp. Proc. (Materials for Optical Limiting II)*, 1997, 479.

4 (*a*) L. W. Tutt and A. Kost, *Nature (London)*, 1992, **356**, 224; (*b*) D. G. McLean, R. L. Sutherland, M. C. Brant, D. M. Brandelik, P. A. Fleitz and T. Pottenger, *Opt. Lett.*, 1993, **18**, 858; (*c*) Y. L. Song, G. Y. Fang, Y. X. Wang, S. T. Liu, C. F. Li, L. C. Song, Y. H. Zhu and Q. M. Hu, *Appl. Phys. Lett.*, 1999, **74**, 332; (*d*) Y. P. Sun and J. E. Riggs, *Int. Rev. Phys. Chem.*, 1999, **18**, 43.

5 (*a*) J. W. Perry, K. Mansour, I. Y. S. Lee, X. L. Wu, P. V. Bedworth, C. T. Chen, D. Ng, S. R. Mardar, P. Miles, T. Wada, M. Tian and H. Sasabe, *Science*, 1996, **273**, 1533; (*b*) J. W. Perry, K. Mansour, S. R. Marder, K. J. Perry, D. Alvarez, Jr. and L. Choong, *Opt. Lett.*, 1994, **19**, 625; (*c*) C. F. Li, L. Zhang, M. Yang, H. Wang and Y. X. Wang, *Phys. Rev. A*, 1994, **49**, 1149.

6 (*a*) S. Shi, W. Ji, S. H. Tang, J. P. Lang and X. Q. Xin, *J. Am. Chem. Soc*., 1994, **116**, 3615; (*b*) P. E. Hoggard, H. W. Hou, X. Q. Xin and S. Shi, *Chem. Mater*., 1996, **8**, 2218.
7 (*a*) C. Zhang, Y. L. Song, B. M. Fung, Z. L. Xue and X. Q. Xin, *Chem. Commun*., 2001, 843; (*b*) C. Zhang, Y. L. Song, G. C. Jin, G. Y. Fang, Y. X. Wang, S. S. S. Raj, H. K. Fun and X. Q. Xin, *J. Chem. Soc., Dalton Trans*., 2000, 1317; (*c*) C. Zhang, Y. L. Song, F. E. Kühn, Y. X. Wang, H. K. Fun and X. Q. Xin, *J. Mater. Chem*., 2002, in press.
8 (*a*) T. H. Wei, D. J. Hagan, M. J. Sence, E. W. Van Stryland, J. W. Perry and D. R. Coulter, *Appl. Phys. B*, 1992, **54**, 46; (*b*) S. Shi, W. Ji and X. Q. Xin, *J. Phys. Chem*., 1995, **99**, 894; (*c*) W. Ji, S. Shi, H. J. Du, P. Ge, S. H. Tang and X. Q. Xin, *J. Phys. Chem*., 1995, **99**, 17 297.
9 (*a*) S. Shi, Z. R. Chen, H. W. Hou, X. Q. Xin and K. B. Yu, *Chem. Mater*., 1995, **7**, 1519; (*b*) Z. R. Chen, H. W. Hou, X. Q. Xin, K. B. Yu and S. Shi, *J. Phys. Chem*., 1995, **99**, 8717; (*c*) H. W. Hou, B. Liang, X. Q. Xin, K. B. Yu, P. Ge, W. Ji and S. Shi, *J. Chem. Soc., Faraday Trans*., 1996, **92**, 2343.
10 (*a*) C. Zhang, Y. L. Song, F. E. Kühn, Y. Xu, X. Q. Xin, H. K. Fun and W. A. Herrmann, *Eur. J. Inorg. Chem*., 2002, 55; (*b*) P. Ge, S. H. Tang, W. Ji, S. Shi, H. W. Hou, D. L. Long, X. Q. Xin, S. F. Lu and Q. J. Wu, *J. Phys. Chem. B*, 1997, **101**, 27; (*c*) H. W. Hou, X. R. Ye, X. Q. Xin, J. Liu, M. Q. Chen and S. Shi, *Chem. Mater*., 1995, **7**, 472.
11 (*a*) H. W. Hou, D. L. Long, X. Q. Xin, X. Y. Huang, B. S. Kang, P. Ge, W. Ji and S. Shi, *Inorg. Chem*., 1996, **35**, 5363; (*b*) H. W. Hou, X. Q. Xin, J. Liu, M. Q. Chen and S. Shi, *J. Chem. Soc., Dalton Trans*., 1994, 3211.
12 (*a*) G. Salane, T. Shibahara, H. W. Hou, X. Q. Xin and S. Shi, *Inorg. Chem*., 1995, **34**, 4785; (*b*) T. Xia, A. Dogariu, K. Mansour, D. J. Hagan, A. A. Said, E. W. Van Stryland and S. Shi, *J. Opt. Soc. Am. B*, 1998, **15**, 1497.
13 (*a*) C. Zhang, Y. L. Song, Y. Xu, H. K. Fun, G. Y. Fang, Y. X. Wang and X. Q. Xin, *J. Chem. Soc., Dalton Trans*., 2000, 2823; (*b*) H. W. Hou, Y. T. Fan, C. X. Du, Y. Zhu, W. L. Wang, X. Q. Xin, M. K. M. Low, W. Ji and H. G. Ang, *Chem. Commun*., 1999, 647.
14 (*a*) A. Muller, E. Diemann and H. Bogge, *Angew. Chem., Int. Ed. Engl*., 1981, **20**, 934; (*b*) R. H. Holm, *Adv. Inorg. Chem*., 1992, **38**, 1; (*c*) M. K. Chan, J. Kim and D. C. Rees, *Science*, 1993, **260**, 792; (*d*) J. Kim and D. C. Rees, *Science*, 1992, **257**, 1677.
15 A. Muller, H. Bogge and U. Schimanski, *Inorg. Chim. Acta*, 1983, **69**, 5.
16 G. Sakane, T. Shibahara, H. W. Hou, Y. Liu and X. Q. Xin, *Trans. Met. Chem*., 1996, **21**, 398.
17 (*a*) J. C. Dyason, L. M. Englehardt, P. C. Healy, C. Pakawatchai and A. H. White, *Inorg. Chem*., 1985, **24**, 1950; (*b*) J. C. Dyason, P. C. Healy, C. Pakawatchai, V. A. Patrick and A. H. White, *Inorg. Chem*., 1985, **24**, 1957; (*c*) E. W. Ainscough, A. G. Bingham, A. M. Brodie and K. L. Brown, *J. Chem. Soc., Dalton Trans*., 1984, 989.
18 C. Zhang, Y. L. Song, Y. Xu, G. C. Jin, G. Y. Fang, Y. X. Wang, H. K. Fun and X. Q. Xin, *Inorg. Chim. Acta*, 2000, **311**, 25.
19 D. L. Long, S. Shi, X. Q. Xin, B. S. Luo, L. R. Chen, X. Y. Huang and B. S. Kang, *J. Chem. Soc., Dalton Trans*., 1996, 2617.
20 M. Sheik-Bahae, A. A. Said, T. H. Wei, D. J. Hagan and E. W. Van Stryland, *IEEE J. Quantum. Electron*., 1990, **26**, 760.
21 S. Shi, H. W. Hou and X. Q. Xin, *J. Phys. Chem*., 1995, **99**, 4050.
22 H. G. Zheng, W. Ji, M. K. M. Low, G. Sakane, T. Shibahara and X. Q. Xin, *J. Chem. Soc., Dalton Trans*., 1997, 2357.
23 S. Speiser and M. Orenstein, *Appl. Opt*., 1988, **27**, 2944.
24 *Optical Electronics in Modern Communications*, ed. A. Yariv, Oxford University Press, New York, 5th edn., 1997.
25 M. Sheik-Bahae, A. A. Said and E. W. Van Stryland, *Opt. Lett*., 1989, **14**, 955.
26 (*a*) G. Y. Fang, Y. L. Song, Y. X. Wang, X. R. Zhang, C. F. Li, L. C. Song and P. C. Liu, *Opt. Commun*., 2000, **183**, 523; (*b*) G. Y. Fang, Y. L. Song, Y. X. Wang, X. R. Zhang, C. F. Li, C. Zhang and X. Q. Xin, *Opt. Commun*., 2000, **181**, 97.
27 J. W. McDonald, G. D. Frieson, L. D. Rosenhein and W. E. Newton, *Inorg. Chim. Acta*, 1983, **72**, 205.
28 G. M. Sheldrick, SADABS, Empirical Absorption Correction Program, University of Göttingen, Germany, 1997.
29 M. Sheik-Bahae, D. C. Hutchings, D. J. Hagan and E. W. Van Stryland, *IEEE J. Quantum. Electron*., 1991, **27**, 1296.